Fluorescent excimers and exciplexes of the purine base derivative 8-phenylethynyl-guanine in DNA hairpins†

Kristen E. Brown, Arunoday P. N. Singh, Yi-Lin Wu, Lin Ma, Ashutosh K. Mishra, Brian T. Phelan, Ryan M. Young, * Frederick D. Lewis * and Michael R. Wasielewski *

The ground- and excited-state electronic interactions between the nucleobase analog 8-(4^0-phenylethynyl) deoxyguanosine, EG, with natural nucleobases and 7-deazaguanine, as well as between adjacent EG base analogs, have been characterized using a combination of steady-state spectroscopy and time-resolved fluorescence, absorption, and stimulated Raman spectroscopies. The properties of the nucleoside EG-H_2 are only weakly perturbed upon incorporation into synthetic DNA hairpins in which thymine, cytosine or adenine are the bases flanking EG. Incorporation of the nucleoside to be adjacent to guanine or deazaguanine results in the formation of short-lived (40–80 ps) exciplexes, the charge transfer character of which increases as the oxidation potential of the donor decreases. Hairpins possessing two or three adjacent EG base analogs display exciton-coupled circular dichroism in the ground state and form long-lived fluorescent excited states upon electronic excitation. Incorporation of EG into the helical scaffold of the DNA hairpins places it adjacent to its neighboring nucleobases or a second EG, thus providing the close proximity required for the formation of exciplex or excimer intermediates upon geometric relaxation of the short-lived EG excited state. The three time-resolved spectroscopic methods employed permit both the characterization of the several intermediates and the kinetics of their formation and decay.

1 Introduction

Fluorescent analogs and derivatives of the nucleobases found in nature have been widely investigated in diverse applications, including DNA sequencing and

Department of Chemistry, Argonne-Northwestern Solar Energy Research (ANSER) Center, Institute for Sustainability and Energy at Northwestern, Northwestern University, Evanston, Illinois 60208-3113, USA. E-mail: ryan.young@northwestern.edu; fdl@northwestern.edu; m-wasielewski@northwestern.edu; Tel: +1-2224-866-3571

† Electronic supplementary information (ESI) available: Additional experimental details for time-resolved spectroscopy and data analysis, hairpin characterization, DFT calculations, time-resolved spectroscopy measurements, and Raman mode assignments.

structural studies, and in photophysical studies, including electron transfer and exciplex and excimer formation.[1,2] Fluorescent bases differ from the natural bases either by minor structural modi cations such as in 2-aminopurine (AP),[3–5] an isomer of adenine, extending the conjugation of the base as in pyrrolocytosine,[6,7] appending a fluorophore such as pyrene to the base,[8] or replacing the entire base with a uorophore.[9] The fluorescent base used most extensively in photophysical studies is AP. Unfortunately, the difference in base pairing for AP vs. adenine (A) with thymine (T) results in perturbation of the duplex structure. This results in the observation of multiple exponential fluorescence decays for duplexes containing a single AP–T base pair, irrespective of the identity of the neighboring base pairs.[10]

A different fluorescent nucleobase, 8-phenylethynylguanine (EG, Chart 1), and its aryl derivatives were prepared and incorporated into nucleosides, oligodeoxynucleotides and duplexes by Firth[11] and by Saito and co-workers.[12,13] The latter group investigated the relative fluorescence intensities of duplexes in which the complementary strand contained a mismatched base opposite EG, and observed enhanced EG fluorescence when opposite T and excimer fluorescence when opposite A. We were attracted to the use of EG as a base analog in studies of photoinduced electron transfer based on the potential use of the oxidized triple bond stretch as a Raman-active signature for its cation radical.[14,15] To our knowledge, the time-resolved spectroscopy of EG-containing duplexes possessing both natural and unnatural flanking bases has not previously been reported. We report here an investigation of the excited-state properties of DNA hairpins possessing a T_3 hairpin linker and either a single EG base with different neighboring bases or two or three stacked sequential EG bases (Chart 1). A combination of steady-state and femtosecond fluorescence upconversion, transient absorption (fsTA), and stimulated Raman (FSRS) spectroscopies reveals the formation of excited states possessing locally excited, charge-transfer exciplex, or excimer characteristics, depending on the identity and oxidation potential of the adjacent base.[16]

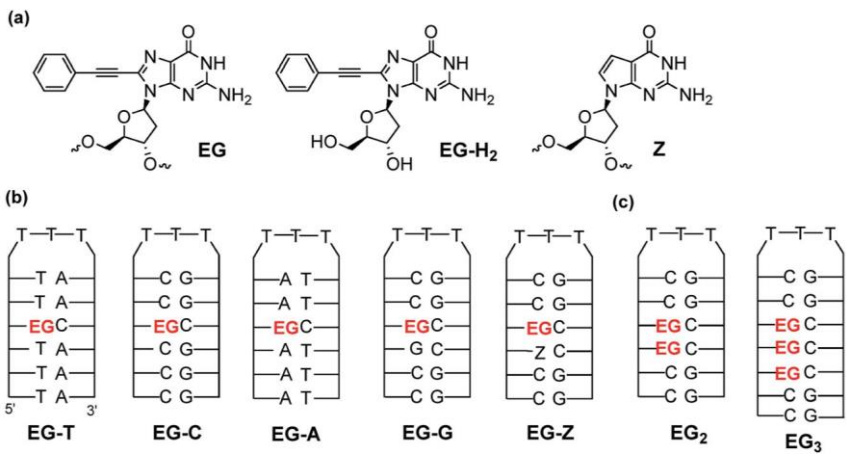

Chart 1 Structures of (a) 8-(4^0-phenylethynyl)deoxyguanosine (EG) and its isolated form (EG-H_2), and the base analog 7-deazaguanosine, Z, (b) EG-X hairpins, and (c) EG_n hairpins.

2 Materials and methods

Reagent grade chemicals were used as received. Flash column chromatography was carried out with SiO_2 (particle size 0.040–0.063 mm, 230–400 mesh) and technical solvents. ^1H and ^{13}C NMR spectra were obtained using a Bruker AVANCE III 500 instrument, and the chemical shifts were determined in ppm relative to the signal of $Si(CH_3)_4$. Residual solvent signals in the NMR spectra were used as an internal reference. High-resolution HR-ESI-MS spectra were obtained using an Agilent 6210 LC-TOF, with the signals reported in m/z units. The nucleoside EG-H_2 was prepared by the method reported by Firth et al.,[11] and the respective DNA conjugates were prepared and purified by HPLC (Fig. S1, ESI†) as previously described.[17] DNA sequences were characterized using MALDI-TOF mass spectrometry, and their steady-state photophysical properties were examined using UV absorption, circular dichroism and fluorescence spectroscopies. All optical measurements of the DNA hairpins were carried out in buffered water (10 mM phosphate, 0.1 M NaCl, pH 7.2). Thermal dissociation temperatures (T_m) and m/z values are reported in the ESI (Table S1†). Fluorescence spectra were acquired using a Jasco fluorescence spectrometer, and the quantum yields (Φ) were determined relative to the quantum yield of quinine sulfate.[18]

Time-resolved fluorescence data were collected at room temperature using a laboratory-constructed fluorescence up-conversion apparatus. The excitation laser source was a commercial direct diode-pumped 100 kHz ampliflier (Spirit 1040-4, Spectra-Physics) which produced the fundamental beam of 1040 nm (350 fs, 4.5 W). The third harmonic of the output was used to pump a non-collinear optical parametric amplifier (Spirit-NOPA-3H, Spectra-Physics) which delivered 320 nm, high repetition rate pulses with pulse durations as short as sub-20 fs (10 nJ per pulse at the sample). The gate pulse was generated with a second harmonic-pumped NOPA (Spirit-NOPA-2H, Spectra-Physics) tuned to 800 nm. The samples were agitated throughout the experiment. The fluorescence was collected and focused into a β-barium borate nonlinear crystal where it was overlapped with the gate pulse. The phase-matching angle was optimized for sum-frequency mixing of the 800 nm gate and the fluorescence at 430 nm. The up-converted light was directed into a monochromator (SPEX 270M, Jobin-Yvon) and detected with a photomultiplier tube. The total instrument response was 150 fs. Details of our fsTA and FSRS experiments have been presented elsewhere.[19,20] The ESI† contains details of the data processing and analysis methods.

3 Results and analysis

3.1. Steady-state spectroscopy

The CD spectra of the EG-X (X ¼ T, C, A, G, and Z) and EG_n (n ¼ 2 or 3) hairpins in aqueous buffer are shown in Fig. 1a and b. All of the EG-containing hairpins exhibit positive bands between 260–300 nm and negative bands between 240– 260 nm, which is consistent with the formation of B-DNA hairpin structures and rules out perturbation of the DNA backbone by the modified EG base.[21] The EG-T, -C and -A hairpins exhibit weak bisignate CD curves, resulting from the weak coupling between EG and their neighboring bases which have different absorption maxima (Fig. 2a).[22] Stronger exciton coupling is observed for EG-G and EG-Z which exhibit more similar absorption maxima for EG and their adjacent purine

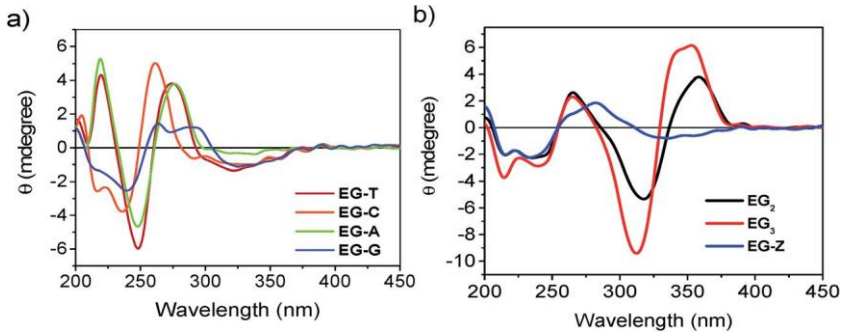

Fig. 1 Circular dichroism spectra of the EG-X hairpins used in this study in phosphate buffer (10 mM phosphate, 0.1 M NaCl, pH 7.2).

bases. The hairpins EG_2 and EG_3 exhibit strong positive bands at 358 and 353 nm, respectively, and negative bands at 317 and 312 nm, respectively, which is characteristic of exciton coupling between identical chromophores.

The UV absorption and fluorescence spectra of $EG\text{-}H_2$ in methanol are shown in Fig. 2a and b, and its spectra in other solvents with varying dielectric constants are shown in Fig. S2 (ESI†). The $EG\text{-}H_2$ spectrum in methanol exhibits an absorption maximum at 320 nm with a vibronic progression of ca. 1800 cm^{-1}. Minimal solvatochromatic response is observed in other solvents. The UV absorption spectra of the EG-X hairpins in phosphate buffer are also shown in Fig. 1a and b. These hairpins exhibit long-wavelength maxima between 330– 335 nm (Table 1), with the weak shoulders at around 355 nm attributed to the EG chromophore, and the short-wavelength maxima between 261–263 nm attributed to the natural nucleobases. The UV spectra of EG_2 and EG_3 (Fig. 1b) exhibit long-wavelength maxima that are blue-shifted with respect to those of $EG\text{-}H_2$ and the

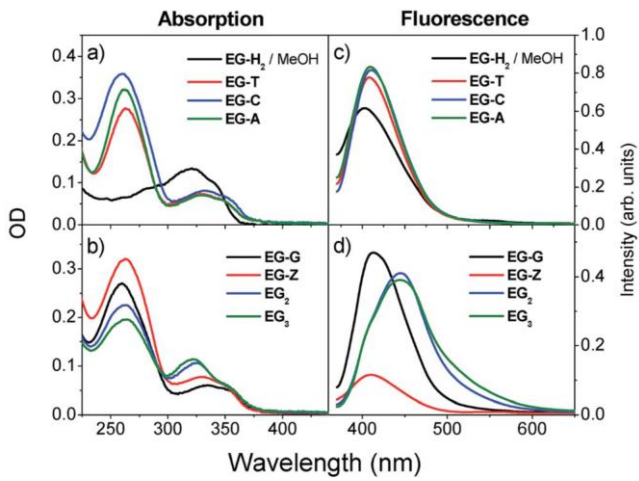

Fig. 2 UV-vis (a and b) and fluorescence (c and d) spectra of the EG-X hairpins (X ¼ T, A, G and zG) and EG_n hairpins (n ¼ 2 or 3) used in this study in phosphate buffer (10 mM phosphate, 0.1 M NaCl, pH 7.2).

Table 1 Neighboring purine (X) oxidation potential, absorption and fluorescence maxima, fluorescence quantum yields (%), fluorescence lifetimes and associated population fractions, as determined by fluorescence up-conversion spectroscopy, and the lifetimes of decay-associated transient absorption spectra in methanol for deoxynucleotide EG and in phosphate buffer (10 mM phosphate, 0.1 M NaCl, pH 7.2) for all hairpins

	E_{ox},[a] V	l_{UV}, nm	l ,[b] nm	F , %	s ,[c] ps	s_{DAS},[d] ps
EG-H_2/MeOH	1.12[e]	320	390	1.3	0.6 (rise), 10.5 (decay)	4.6, 16
EG-T	—	330	410	1.4	8.0 (55%), 43 (45%)	4.4, 40
EG-C	—	332	410	1.4	0.4 (rise), 22.7 (decay)	3.8, 28
EG-A	1.36	330	414	1.5	18 (55%), 55 (45%)	6.9, 42
EG-G	1.11	336	408	0.7	3.2 (49%), 37 (51%)	2.1, 14, 73
EG-Z	0.81e	331	410	0.2		0.3, 3.3, 26, 68
EG_2	1.12	325	444	0.8		0.3, 3.1, 30, 490, 2900
EG_3		321	444	0.8		0.7, 5.1, 71, 670, 4110

[a] V vs. Ag/AgCl in phosphate buffer (pH 7.2) with 0.1 M NaCl from ref. 16. [b] l_{ex} ¼ 320 nm. [c] Determined from uorescence up-conversion spectroscopy. The ts for EG-Z, EG_2 and EG_3 were of poor quality and are not reported (see text). [d] Determined from transient absorption spectroscopy. [e] V vs. SCE in DMF from ref. 15.

other EG-X hairpins (Table 1). Density functional theory (DFT) calculations for the EG chromophore were carried out at the B3LYP/6-31G(d) level (see ESI† for details).[23] The long-wavelength absorption band is assigned to a long-axis-polarized allowed HOMO–LUMO transition between delocalized p-orbitals (Fig. S3 and Tables S2 and S3, ESI†).

The fluorescence spectra of the nucleoside EG-H_2 in methanol and the hair-pins in aqueous buffer are shown in Fig. 2c and d. In MeOH, the spectral maximum appears at 390 nm and the fluorescence quantum yield (F) is ca. 1.3%. The fluorescence maxima (l) for the EG-X and EG_n hairpins are red-shifted with respect to that for EG-H_2, however the fluorescence quantum yields for the hairpins EG-X (X ¼ C, T, or A) are similar to that for EG-H_2 in polar protic and aprotic solvents (Fig. S2c, ESI†). The value of F in the non-polar aprotic solvent THF is significantly higher (F ¼ 16%), which is consistent with the report of Saito and co-workers.[12,13] Somewhat lower values of F are observed for EG-G, EG-Z, EG_2 and EG_3, and the fluorescence spectra of EG_2 and EG_3 are red-shifted and broadened. The values of F and l are summarized in Table 1.

3.2. Time-resolved spectroscopies

3.2.1. Fluorescence up-conversion. Fluorescence decay traces for the nucleoside EG-H_2 in methanol and THF and for the EG-X hairpins (X ¼ T, -C, -A or -G) in aqueous buffer, determined at 430 nm following 320 nm pulsed laser excitation, are shown in Fig. S4 (ESI†). The decay of EG-H_2 is best fitted as a single exponential with a decay time of 10.5 ps following a 600 fs rise, which is commensurate with the low (1%) quantum yield of emission. In THF, the fluorescence decay of EG-H_2 is biexponential, with s_1 ¼ 13.6 ps and s_2 ¼ 220 ps comprising 85% and 15% of the decay pro le, respectively. The EG-X hairpins, with the exception of EG-C, exhibit dual exponential decays with short decay times (3–20 ps) that are

similar to the decay time of EG-H_2 in methanol, followed by a longer (37–55 ps) decay. EG-C exhibits a single 23 ps decay following a fast rise, which is similar to that of EG-H_2 in methanol. The fluorescence decays of EG-Z, EG_2 and EG_3 were of poor quality, which is plausibly due to the low fluorescence intensity at 430 nm and the presence of multiple intermediates (see below). The decay times obtained from the exponential fits of the transient data shown in Fig. S4 (ESI†) are summarized in Table 1.

3.2.2. Femtosecond transient absorption spectroscopy. The femtosecond transient absorption spectra of EG-H_2 in methanol and the hairpins EG-C and EG-G acquired a er 350 nm excitation are shown in Fig. 3. These spectra are dominated at short delay times by a single band between 450–600 nm. Global analysis of the transient absorption data with bi- or tri-exponential decays yields two decay-associated spectra (DAS) with similar maxima but differing in their band shapes and lifetimes. The DAS are shown as insets in Fig. 3. The decay times for EG-H_2 and EG-C are consistent with those reported in our prior study.[15] The fast component has a maximum at 506 nm and a decay time of 2–4 ps, accompanied by a growth in intensity near 645 nm which is clearly seen in the case of EG-H_2. The longer-lived component (tens of ps) exhibits a blue-shifted maximum at 495 nm and a tail that extends beyond 700 nm (Fig. 3a). The relaxation dynamics of EG-H_2 are highly solvent dependent. The fsTA data for EG-H_2 in aqueous buffer

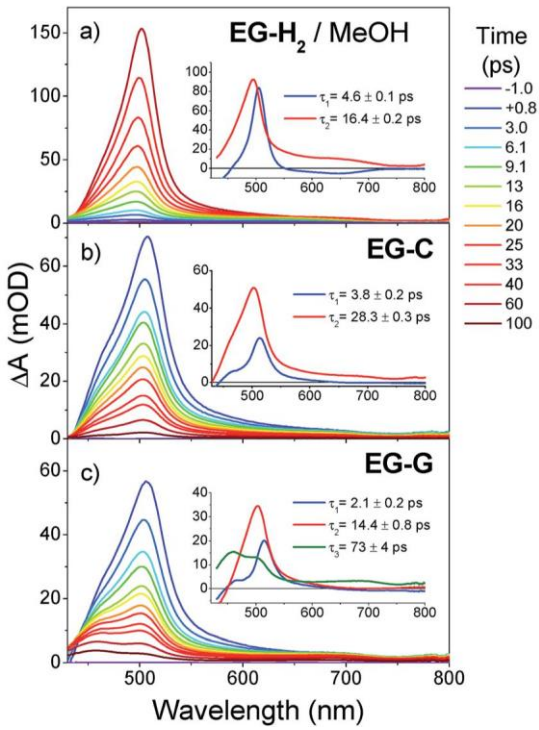

Fig. 3 Transient absorption spectra for (a) nucleoside EG in methanol and the hairpins (b) EG-C and (c) EG-G in phosphate buffer (10 mM phosphate, 0.1 M NaCl, pH 7.2) following excitation by a 350 nm, 60 fs pulse (1.0 mJ per pulse). Insets: decay-associated spectra following multi-wavelength global fitting.

(Fig. S5, ESI†) show two short components with similar DAS to those in methanol, but with lifetimes that are almost twice as short (2 and 9 ps, compared to 5 and 16 ps in methanol). In THF, both the fluorescence up-conversion and the transient absorption data demonstrate more complex decays; a fast 2 ps decay is accompanied by a shift in the absorption maximum from 510 to 497 nm. The first two DAS resemble the spectra obtained in methanol but have longer decay times. In addition there is a third broad absorption between 450–500 nm that has a decay time of 207 ps, which likely arises from the same population that gives the long-lived emission (Fig. S4, ESI†). Similar behavior is observed in acetonitrile, with faster initial components (1 and 5 ps) and a slower 240 ps decay (Fig. S5, ESI†).

The transient absorption spectra for EG-C, -T and -A are shown in Fig. 3b and S6 (ESI†). They exhibit DAS and short-lived decay components that are similar to that of $EG\text{-}H_2$, however their long decay times are longer than that of $EG\text{-}H_2$ in methanol (Table 1). The long-lived components of the DAS are also similar to those extracted from the fluorescence up-conversion data (Fig. S4, ESI†). The fsTA spectra of EG-G (Fig. 3c and S7a, ESI†) exhibit two short-lived DAS components that are similar in band shape to those of EG-C, and a third, longer-lived component which has band maxima at 455 nm and 700 nm. The differences between the transient spectra of the hairpin EG-Z and those of the hairpins EG-C, -T and -A are even more pronounced (Fig. 4a and S7b, ESI†), with new bands appearing with maxima at around 460 and 680 nm. The initially formed 508 nm band is broader and shorter-lived than the initial transients of the other EG-X hairpins. The DAS for these processes in EG-Z exhibit both decreases at around 500 nm and rises near 460 and 680 nm, which matches the observed behavior of the spectra. The lifetimes of these first two DAS are 0.3 and 3.3 0.3 ps, respectively. Following these, the 460 and 680 nm peaks decay bi-exponentially, with the major and minor components exhibiting decay times of 26 1 ps and 68 4 ps, respectively.

The transient absorption spectra for the hairpins EG_2 and EG_3 (Fig. 4b and c and Fig. S8a and b, ESI†) exhibit even larger divergence from those of EG-C, -T and -A. As in the case of EG-Z, both EG_2 and EG_3 display strong bands at 450 and 680 nm after a few ps. However, these bands exhibit longer lifetimes than those observed for EG-Z. Similarly, the five DAS needed to t the spectra of EG_2 and EG_3 exhibit significantly longer decay times than those of EG-Z. In EG_2, the decay-associated fitting shows that the initially formed band with a maximum near 508 nm decays bi-exponentially, accompanied by a growth near 450 nm and a broad feature centered at 680 nm. This process occurs with 0.3 and 3.0 ps time constants. EG_2 also exhibits a slower, 30 1 ps decay of the 500 nm band, with a concomitant increase of the amplitude near 430 nm, but growth near 680 nm is not observed in this component. The resulting intermediate exhibits peaks at 450 nm and 685 nm that dominate the spectra and which decay bi-exponentially, with the major and minor components exhibiting decay times of 490 10 ps and 2900 170 ps, respectively.

The dynamics and DAS for EG_3 are quite similar to those for EG_2, but with even longer-lived states. The 508 nm band is rapidly replaced by features at 450 and 680 nm, similar to those of EG_2, but with longer time constants of 0.7 0.3 and 5.1 0.3 ps, respectively. Further decay of the 508 nm band occurs over 71 4 ps with no associated growth of the 680 nm band. The resultant intermediate again

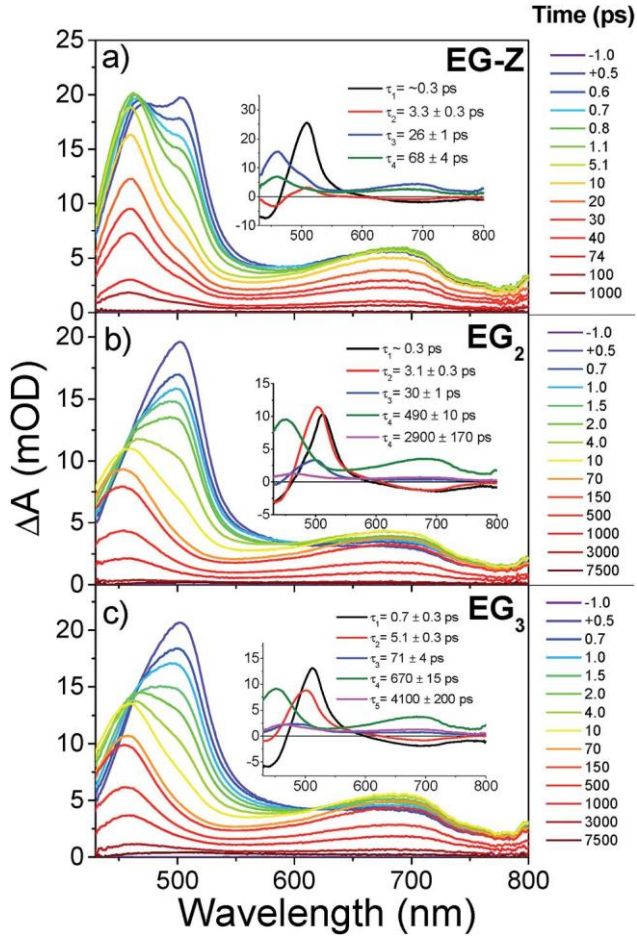

Fig. 4 Transient absorption spectra for the hairpins (a) EG-Z, (b) EG_2 and (c) EG_3 in phosphate buffer (10 mM phosphate, 0.1 M NaCl, pH 7.2) following excitation by a 350 nm, 60 fs pulse (1.0 mJ per pulse). Insets: decay-associated spectra following multi-wave-length global fitting.

decays bi-exponentially, with decay times of 670 15 and 4100 200 ps. The lifetimes extracted from the decay-associated fitting are given in Table 1.

3.2.3. Femtosecond stimulated Raman spectroscopy. The FSRS spectrum of EG-H_2 in methanol, acquired with a 480 nm Raman pump following 350 nm actinic excitation, is shown in Fig. S9a (ESI†) and exhibits bi-exponential decay with 1 and 13 ps decay times. Mode assignments are given in Table S4 (ESI†). The decay-associated Raman spectra exhibit the same general shape, with subtle changes in the relative intensities of the transitions near 1000 cm^{1} (Fig. S9a, ESI†). We also observe a broadening and small shift of the C^C stretch at 2106 cm^{1}. These differences indicate that the coupling of these vibrations to the 480 nm electronic transition changes as the state evolves following excitation. The FSRS spectra of the hairpins EG-C, EG-G, EG-Z and EG_2 are shown in Fig. 5. The two highest frequency bands for EG-C and EG-G are narrower and more intense

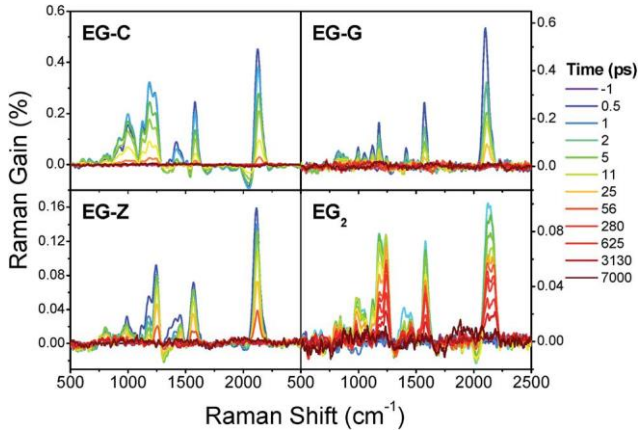

Fig. 5 Femtosecond stimulated Raman spectra of the hairpins EG-C, EG-G, EG-Z and EG_2 following 350 nm actinic excitation and collection using a 480 nm Raman pump.

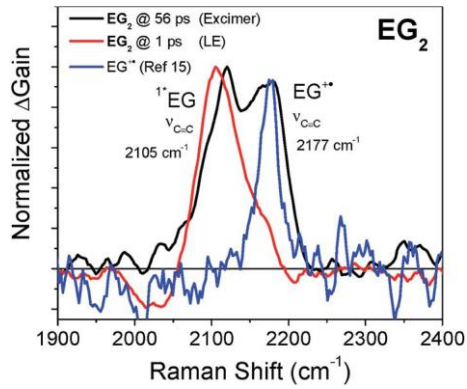

Fig. 6 Overlay of the normalized FSRS spectrum of EG_2 at 56 ps (black curve) with the ^{1*}EG spectrum of EG_2 at 1 ps (red curve) and the EG^{+}c spectrum (blue curve) from ref. 15.

than those of the other hairpins. The bands of EG-Z are notably less intense, broader and shifted to a lower frequency. The EG_2 bands are most distinct, with the highest frequency band split into two peaks near 2110 and 2180 cm^{-1} that decay over several nanoseconds (Fig. 6), in keeping with the long decays observed in the fsTA experiments (Table 1). Additional variations in peak intensities are observed in the lower frequency 750–1500 cm^{-1} region of EG_2 (Fig. 5), thus demonstrating its unique behavior relative to the other hairpins. The strong coupling between nucleobases complicates the computation and assignment of the excited-state Raman bands of these hairpins.

4 Discussion

4.1. Excited-state dynamics of EG-H_2

The excited-state behavior of EG-H_2 in MeOH can be summarized as shown in Scheme 1a. The bi-exponential evolution of the fsTA is attributed to the geometric

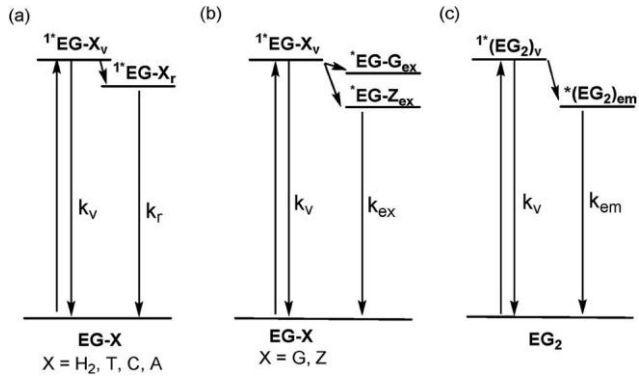

Scheme 1 Schematic for excited-state evolution showing the formation and decay of vertical and relaxed states for (a) nucleoside EG-H_2 and the hairpins EG-C, -T and -A, (b) exciplex states for EG-G and EG-Z and (c) the excimer state for EG_2. The decay times are given in Table 1. Assignments of the fast and slow decay components are discussed in the text.

relaxation of the vertical excited state ^{1*}EG-H_{2v} to the relaxed excited state ^{1*}EG-H_{2r}. Indeed, there may be significant nuclear rearrangement from the vertically accessed state during this time, resulting in the observed bi-exponential decay. Such behavior has been recently proposed to explain the photophysics of 8-vinylguanine (VG).[24] The fluorescent vertical state of VG can cross a low barrier to access a part of the potential energy surface that more closely resembles the L_a state of unsubstituted guanine,[25] where rapid internal conversion or motion through a conical intersection (CI) can be accessed.[26] CIs have been established as the primary decay pathway for photoexcited natural nucleobases.[27] A similar twisting of the phenylethynyl substituent relative to the guanine core may explain the changes in the Raman spectrum discussed above. Notably, computational work predicts that the vertical state of VG exhibits a higher degree of charge-transfer (CT) character than the relaxed non- fluorescent state.[24] A similar relaxation mechanism for EG-H_2 would explain the observed trends in the fluorescence quantum yield F with solvent polarity and hydrogen bonding. In their original work, Saito and co-workers noted that the fluorescence of EG-H_2 is solvent-dependent, being weaker and red-shifted in the polar solvents acetonitrile and methanol than in the less polar solvent ethyl acetate.[12] A higher, solvent-dependent barrier to accessing the L_a-like region of the potential energy surface in EG-H_2 could result in a reduction of the rate of approach to the CI, thereby increasing the fluorescence quantum yield. This mechanism is also consistent with the multi-exponential decay observed in both polar and non-polar solvents, and the increased complexity of the decay dynamics with increasing solvent polarity (Fig. S4 and S5, ESI†). The observation of the 200 ps emissive state of EG-H_2 in THF might suggest that the barrier to accessing the L_a-like state is modulated via hydrogen bonding; the decays are relatively fast in the protic solvent MeOH but are slowed in the aprotic solvents THF and acetonitrile.

4.2. Hairpins with flanking natural nucleobases

Saito et al. investigated the fluorescence properties of duplexes possessing a p-acetyl substituted EG flanked by either C or T bases with matched or mismatched

bases in the complementary strand opposite EG, and found that the fluorescence intensity for the mismatch of EG with T was higher than that for a mismatch with A or G or base pairing with C.[13] The hairpins in our study have the EG base paired with C; only the identity of the flanking base pairs is varied (Chart 1). The small shifts in the UV and fluorescence maxima of EG-C and EG-T when compared to EG-H_2 (Fig. 1a) and the weak negative long-wavelength bands in their CD spectra (Fig. 2a) are indicative of weak ground-state interactions of EG with the neigh-boring pyrimidine bases.[28]

The time-resolved spectroscopy data suggest that the excited-state behavior of the EG-C, EG-T and EG-A hairpins is similar in some respects to that of EG-H_2, thus implying minimal excited-state interaction with the neighboring nucleo-bases. The hairpins EG-C and EG-T have F values and short-lived components of fluorescence and transient absorption decay that are similar to those for EG-H_2 (Table 1). The long-lived components of the fluorescence and transient absorption decay of EG-C are longer than those of EG-H_2 and are assigned to the decay of the relaxed excited state ^{1*}EG-X_r via a mechanism similar to that for EG-H_2 dis-cussed above (Scheme 1a). The phenylethynyl group extends into the minor groove adjacent to the guanosine deoxyribose, and thus decay of the relaxed excited states of EG-T and -C may be slowed relative to EG-H_2 by the ordered solvent within the minor groove as well as base pairing and base stacking within the DNA scaffold. The FSRS spectra for EG-C and EG-H_2 (Fig. 5 and S9a, ESI†) exhibit the same relative band structure and shift in the ethynyl stretch at longer times, which suggests that the relaxation process is not substantially perturbed by the base-paired structure. Although EG-A deploys purine bases on both sides of the EG nucleoside, it possesses ground- and excited-state properties that are similar to those of EG-C and -T. Based on the difference in the oxidation potentials of A and EG (Table 1), their HOMO energies are likely still too disparate in energy to significantly mix, thus resulting in their similar excited-state dynamics with only a small extension of the excited-state lifetime (Table 1). The excited-state behavior of the hairpins EG-C, -T and -A is summarized in Scheme 1a.

The CD spectrum of EG-G exhibits stronger exciton coupling in the 300– 350 nm region than for the spectra of EG-C, -T and -A (Fig. 1a). More pronounced interactions also appear in the excited-state behavior of EG-G, even though it possesses a single flanking purine base rather than two as is the case for EG-A. The absorption maximum is also shifted to 336 nm, which is the longest wave-length in the series (Table 1). While the maximum of the dominant emission of EG-G is similar to those of EG-C, -T and -A, its fluorescence is more strongly quenched, with F ¼ 0.7%, which is the lowest of the sequences possessing flanking natural bases. It also exhibits weak long-wavelength fluorescence extending beyond 550 nm, which is attributed to a weakly fluorescent exciplex (Fig. 2d). Accordingly, both the vertical and relaxed excited states of EG-G in the fluorescence up-conversion measurements decay more rapidly than those of EG-A. We attribute this behavior to the quenching of the fluorescent ^{1*}EG-G_v state via the formation of the weakly- fluorescent exciplex (Scheme 1b).

The transient absorption spectra of EG-G (Fig. 3c) support this mechanism. These spectra exhibit two short-lived components of the DAS that are similar in band shape to those of EG-C, and a third, longer-lived component which has a band maximum at 455 nm as well as at 700 nm. This state decays with a 73 ps lifetime, which is longer than the longest time observed by time-resolved

fluorescence. We assign this state to the weakly emissive exciplex ^{1*}EG-G$_{ex}$. Since EG and G have similar oxidation potentials, this intermediate is best viewed as a "heteroexcimer" with resonance contributions from both of the charge resonance states EG $^{-}$G^{+} and EG^{+}-G , as well as the locally excited state ^{1*}EG-G.[29] The similar redox potentials of EG and G[15] allow for sufficient mixing to form an exciplex with moderate CT character; the extended 70 ps lifetime reflects the stabilization afforded by this mixing. The lower LUMO energy for EG vs. G makes it likely that EG $^{-}$G^{+} is an important charge-resonance contributor. However, we have also demonstrated[15] that EG^{+}c absorbs at 460 nm with a spectral width similar to that shown in Fig. 3c, so this absorption may indicate a contribution from that charge-resonance state. The perturbation of the low frequency portion of the EG-G FSRS spectra relative to EG-H$_2$ also indicates a minor impact of excited-state coupling between EG and G.

In summary, ^{1*}EG does not appear to strongly interact with the natural nucleobases, with the exception of guanine where the HOMO energy levels are the most favorable for exciplex formation (vide infra). In the case of EG-C, -T and -A, the solvent and nuclear relaxation of the vertical excited state yields a longer-lived relaxed singlet state, with minimal electronic mixing between the locally excited state of EG and the flanking bases (Fig. 1a). In the case of EG-G, the vertical excited state forms a weakly fluorescent exciplex that possesses a small amount of charge-transfer character (Fig. 1b). Exciplex formation with G might compete with the formation of a relaxed EG-G or -C complex, thus accounting for the several components of the fsTA. However, in the absence of direct observation of additional intermediates, only the exciplex is shown in Fig. 1b.

4.3. Hairpins with flanking deazaguanine

We next consider the excited-state behavior of ^{1*}EG when it is adjacent to the modified nucleobase Z. Unlike the other EG-X conjugates, EG-Z exhibits strong exciton-coupled CD bands at long wavelengths (Fig. 1b). The absorption and fluorescence maxima for EG-Z are similar to those for EG-T and -C, however, its value of F is markedly smaller and it exhibits a weak fluorescence band near 560 nm, similar to that of EG-G, which is attributed to exciplex fluorescence (Fig. 2d). The values of F and the short- and long-lived components of s for the EG-X hairpins with flanking purines follow the order of purine oxidation potential: Z < G < A (Table 1). These data corroborate the assertion that purines can form exciplexes with EG, with the extent of the CT character being determined by the purine oxidation potential. Similar behavior has been observed for the fluorescent base aminopurine in its dinucleotides, with the most efficient quenching being observed when AP is stacked with G.[30,31]

The transient absorption spectra of EG-Z (Fig. 4a) also differ in appearance from those of the other EG-X hairpins (Fig. 3b and c). This difference is attributed to the greater extent of charge-transfer character in the exciplex as a consequence of the increased contribution of the charge-resonance state EG $^{-}$Z^{+} to the resonance description of the exciplex. The initially formed ^{1*}EG-Z$_v$ state (l_{max} 500 nm) decays via rapid exciplex formation, leading to the exciplex ^{1*}EG-Z$_{ex}$ with maxima near 460 and 680 nm without the formation of a relaxed singlet state (Scheme 1c). The prompt decay of the weak fluorescence and the 500 nm DAS is attributed to the decay of the vertical singlet state, whereas the slower decays of

the fluorescence and the 460 and 680 nm DAS are attributed to the exciplex. The dual exponential decay of the exciplex plausibly arises as a result of the solvent or nuclear relaxation of the polar exciplex within the solvated DNA duplex. Alter-natively, the non-rigid DNA backbone may simply lead to a distribution of conformers with variations in the p-stacking and subsequently the exciplex decay rates.[5]

4.4. Hairpins with adjacent phenylethynylguanine

The hairpins EG_2 and EG_3 which possess two and three stacked EG bases, respectively (Chart 1), exhibit strong electronic interactions in both the ground and excited states. The CD spectra of these hairpins exhibit strong exciton coupling unlike that of the EG-X hairpins (Fig. 1a and b). The blue-shifted CD maxima and minima and increased CD intensity for EG_3 and EG_2 are similar to those for duplexes that possess helical arrays of the modified nucleobase pyrollocytosine, which has a calculated torsion angle of 30 between the long axes of its chromophores.[7] The long-wavelength absorption maxima of EG_2 and EG_3 (Fig. 2b) are blue-shifted with respect to that of EG-G, with the shift being largest for EG_3, however, the fluorescence maxima of EG_2 and EG_3 exhibit the largest redshifts (Fig. 2d). Less pronounced changes in the UV band shape and similar, but weaker, EC-CD spectra have been reported for DNA duplexes possessing adjacent 2-aminopurine[32] and pyrrolocytosine[7,33] chromophores. The more intense EC-CD spectra for adjacent EG no doubt reflect the fully allowed nature of its lowest energy p–p* transition (Fig. S3†). The fluorescence spectra of EG_2 and EG_3 are broadened and red-shifted with respect to those of the natural-base EG-X hairpins (Fig. 1), which is consistent with their assignment to excimer or over-lapping monomer and excimer fluorescence. The values of F and both the short-and long-lived components of s are smaller than those for EG-C (Table 1), which is as expected for an excimer state wherein non-radiative decay dominates.[34,35] Since EG_2 and EG_3, like EG-C, have flanking cytosine bases, the reduction in F reflects the non-radiative decay of the $^{1*}EG_{2em}$ excimer rather than the quenching of excimer fluorescence.

The fsTA DAS of EG_2 and EG_3 are similar in appearance to those of EG-Z, thus suggesting similar relaxation dynamics (Fig. 4). However, the lifetimes of the longest states are significantly longer for EG_2 than for EG-Z (2.9 ns vs. 68 ps), as is typical for aromatic hydrocarbon excimers within DNA.[35,36] The observation of two absorption maxima with a large spectral separation for the transient absorption spectrum of an excimer has previously been observed for perylenediimide dimers, and was attributed to the non-aligned geometry of their transition dipoles.[37] Alignment of the transition dipoles of adjacent bases within B-DNA would require substantial torsional motion of the duplex and is therefore unlikely. Transient absorption measurements of p-stacked dimers have shown that ultrafast excimer formation can be followed by an increase in the oscillator strength of excimer absorption on the ps timescale attributed to structural relaxation of the exci-mer.[38–40] The ultrafast component of the growth of the exciplex feature would thus reflect the excimer formation process, while the slower growth may represent a similar structural relaxation event. The excited-state properties of EG_2 and EG_3 are similar but not identical, as would be expected for excimers possessing two and three identical chromophores. However, the environment of the EG

chromophores differs within the two hairpins, with the excimer from EG_2 possessing two cytosine neighbors and the excimer from EG_3 possessing either of two possible cytosines and one EG as neighbors.

The excited-state behavior of EG_2 and EG_3 can be summarized as shown in Scheme 1c. Despite the observation of strong exciton coupling in the UV and CD spectra, the transient absorption spectra of EG_2 and EG_3 (Fig. 4a–c) immediately following excitation are similar to those of the EG-X hairpins and are thus assigned to the vertical excited state of a single EG chromophore. Again, the multiple formation rates extracted from the decay-associated fitting of the fsTA data are consistent with bi-exponential fluorescence decay. The initially populated short-lived fluorescent state can either form the fluorescent relaxed state $^{1*}EG–EG_r$ or the long-lived excimer $^{*}EG–EG_{ex}$.

The FSRS spectra of EG_2 exhibit interesting features for the EG excimer. The lower intensity of the EG_2 FSRS spectra compared to those of the other hairpins at similar concentrations is consistent with previously observed excited-state inter-actions between cofacial chromophores, which have been demonstrated to exhibit substantially weakened and broadened band intensities.[41] Uniquely, the broad EG_2 ethynyl stretch, initially at 2140 cm^{-1}, bifurcates into two well resolved bands at 2105 and 2177 cm^{-1} within the rst 10 ps. This change is accompanied by the loss of intensity in the 1178 cm^{-1} C–N stretching mode associated with the decay of the locally excited $^{1*}EG$ state into the EG–EG excimer. Importantly, the 2177 cm^{-1} band is of a similar frequency to that of $EG^{+}c$ observed in our previous work.[15] Fig. 6 shows an overlay of the EG_2 excimer FSRS spectrum and that of $EG^{+}c$ adapted from ref. 15, along with the $^{1*}EG$ spectrum in the ethynyl stretch region. The simultaneous appearance of transitions associated with both $EG^{+}c$ and $^{1*}EG$ is consistent with the classic picture of an excimer as the mixture of those two electronic states, and suggests a substantial contribution from the charge-resonance configuration in the excimer.[41] Overall, the high CT-character of the EG excimer offers an interesting probe into the electronic interactions within excimers and allows us to track their structural evolution over time.

5 Concluding remarks

The fluorescent base analog 8-phenylethynylguanine (EG) has proven to be a versatile probe of ground- and excited-state interactions with flanking nucleo-bases in fully base-paired DNA hairpins. Base pairing with C places EG at the edge of the minor groove of B-DNA where it does not disrupt the base-paired structure. The fluorescence quantum yields and decay times of the hairpins possessing flanking T, C and A bases in aqueous buffer are similar to those for the nucleoside in methanol, which is indicative of weak ground- and excited-state interactions between EG and these bases. The excited states of these hairpins decay via fluorescence and non-radiative pathways from both vertical and relaxed singlet states. $^{1*}EG$ forms charge transfer-stabilized exciplexes with G and Z, with the extent of charge separation increasing as the purine oxidation potential decreases. When paired with itself, $^{1*}EG$ forms an excimer, having significantly longer lifetimes than its exciplexes with G or Z. The EG excimer appears to have significant CT character, as evidenced by the observation of both $^{1*}EG$ and $EG^{+}c$ bands in the FSRS spectra.

The interplay between electron transfer and exciplex formation remains an area of deep interest.[42,43] The work discussed above strongly highlights the continued need to develop new systems and techniques to probe fundamental interactions between cofacial, electron-rich molecules in functional systems.

Acknowledgements

This material is based upon work supported by the U.S. Department of Energy, Office of Science, Office of Basic Energy Sciences, Chemical Sciences, Geo-sciences, and Biosciences Division under the Awards DE-FG02-96ER14604 (F. D. L.) and DE-FG02-99ER14999 (M. R. W.).

References

1 J. N. Wilson and E. T. Kool, Org. Biomol. Chem., 2006, 4, 4265–4274.
2 R. W. Sinkeldam, N. J. Greco and Y. Tor, Chem. Rev., 2010, 110, 2579–2619.
3 C. Wan, T. Fiebig, O. Schiemann, J. K. Barton and A. H. Zewail, Proc. Natl. Acad. Sci. U. S. A., 2000, 97, 14052–14055.
4 T. Gelot, P. Tour´on-Touceda, O. Cr´egut, J. L´eonard and S. Haacke, J. Phys. Chem. A, 2012, 116, 2819–2825.
5 V. A. Spata, W. Lee and S. Matsika, J. Phys. Chem. Lett., 2016, 7, 976–984.
6 K. C. Thompson and N. Miyake, J. Phys. Chem. B, 2005, 109, 6012–6019.
7 P. P. Neelakandan, M. McCullagh, G. C. Schatz and F. D. Lewis, J. Phys. Chem. B, 2012, 116, 5199–5204.
8 A. Trifonov, M. Raytchev, I. Buchvarov, M. Rist, J. Barbaric, H.-A. Wagenknecht and T. Fiebig, J. Phys. Chem. B, 2005, 109, 19490–19495.
9 E. T. Kool, Acc. Chem. Res., 2002, 35, 936–943.
10 A. Dallmann, L. Dehmel, T. Peters, C. Mugge,¨ C. Griesinger, J. Tuma and N. P. Ernsting, Angew. Chem., Int. Ed., 2010, 49, 5989–5992.
11 A. G. Firth, I. J. S. Fairlamb, K. Darley and C. G. Baumann, Tetrahedron Lett., 2006, 47, 3529–3533.
12 Y. Shinohara, K. Matsumoto, K. Kugenuma, T. Morii, Y. Saito and I. Saito, Bioorg. Med. Chem. Lett., 2010, 20, 2817–2820.
13 Y. Saito, K. Kugenuma, M. Tanaka, A. Suzuki and I. Saito, Bioorg. Med. Chem. Lett., 2012, 22, 3723–3726.
14 Y.-L. Wu, K. E. Brown, D. M. Gardner, S. M. Dyar and M. R. Wasielewski, J. Am. Chem. Soc., 2015, 137, 3981–3990.
15 K. E. Brown, A. P. N. Singh, Y.-L. Wu, A. K. Mishra, J. Zhou, F. D. Lewis, R. M. Young and M. R. Wasielewski, J. Am. Chem. Soc., 2017, DOI: 10.1021/jacs.7b06998.
16 A. S. Jalilov, S. Patwardhan, A. Singh, T. Simeon, A. A. Sarjeant, G. C. Schatz and F. D. Lewis, J. Phys. Chem. B, 2014, 118, 125–133.
17 F. D. Lewis, T. Wu, X. Liu, R. L. Letsinger, S. R. Green eld, S. E. Miller and M. R. Wasielewski, J. Am. Chem. Soc., 2000, 122, 2889–2902.
18 W. H. Melhuish, J. Phys. Chem., 1961, 65, 229–235.
19 R. M. Young, S. M. Dyar, J. C. Barnes, M. Jur´ı˘cek, J. F. Stoddart, D. T. Co and M. R. Wasielewski, J. Phys. Chem. A, 2013, 117, 12438–12448.
20 K. E. Brown, B. S. Veldkamp, D. T. Co and M. R. Wasielewski, J. Phys. Chem. Lett., 2012, 3, 2362–2366.

21 K. E. V. Holde, W. C. Johnson and P. S. Ho, Principles of Physical Biochemistry, Pearson/Prentice Hall, 2006.
22 N. Berova and K. Nakanishi, in Circular Dichroism, ed. N. Berova, K. Nakanishi and R. W. Woody, Wiley-VCH, New York, 2000.
23 M. J. Frisch, G. W. Trucks, H. B. Schlegel, G. E. S. M. A. Robb, J. R. Cheeseman, G. Scalmani, V. Barone and G. A. Petersson, Gaussian 09, Gaussian, Inc., Wallingford CT, 2009.
24 M. A. Kochman, M. Pola and R. J. D. Miller, J. Phys. Chem. A, 2016, 120, 6200–6215.
25 A. F. El-Yazbi, A. Palech and G. R. Loppnow, J. Phys. Chem. A, 2011, 115, 10445– 10451.
26 C. T. Middleton, K. d. L. Harpe, C. Su, Y. K. Law, C. E. Crespo-Hern´andez and B. Kohler, Annu. Rev. Phys. Chem., 2009, 60, 217–239.
27 C. E. Crespo-Hernandez, B. Cohen, P. M. Hare and B. Kohler, Chem. Rev., 2004, 104, 1977–2019.
28 F. D. Lewis, L. Zhang, X. Liu, X. Zuo, D. M. Tiede, H. Long and G. S. Schatz, J. Am. Chem. Soc., 2005, 127, 14445–14453.
29 M. Ottolenghi, Acc. Chem. Res., 1973, 6, 153–160.
30 O. F. A. Larsen, I. H. M. van Stokkum, F. L. de Weerd, M. Vengris, C. T. Aravindakumar, R. van Grondelle, N. E. Geacintov and H. van Amerongen, Phys. Chem. Chem. Phys., 2004, 6, 154–160.
31 O. J. G. Somsen, L. B. Keukens, M. N. de Keijzer, A. van Hoek and H. van Amerongen, ChemPhysChem, 2005, 6, 1622–1627.
32 N. P. Johnson, W. A. Baase and P. H. von Hippel, Proc. Natl. Acad. Sci. U. S. A., 2004, 101, 3426–3431.
33 N. P. Johnson, W. A. Baase and P. H. von Hippel, Proc. Natl. Acad. Sci. U. S. A., 2005, 102, 7169–7173.
34 K. E. Brown, W. A. Salamant, L. E. Shoer, R. M. Young and M. R. Wasielewski, J. Phys. Chem. Lett., 2014, 5, 2588–2593.
35 E. A. Chandross and H. T. Thomas, J. Am. Chem. Soc., 1972, 94, 2421–2424.
36 F. D. Lewis, T. Wu, E. L. Burch, D. M. Bassani, J.-S. Yang, S. Schneider, W. Jaeger and R. L. Letsinger, J. Am. Chem. Soc., 1995, 117, 8785–8792.
37 P. P. Neelakandan, T. A. Zeidan, M. McCullagh, G. C. Schatz, J. Vura-Weis, C. H. Kim, M. R. Wasielewski and F. D. Lewis, Chem. Sci., 2014, 5, 973–981.
38 J. Sung, P. Kim, B. Fimmel, F. Wurthner¨ and D. Kim, Nat. Commun., 2015, 6, 8646.
39 C. M. Mauck, R. M. Young and M. R. Wasielewski, J. Phys. Chem. A, 2017, 121, 784–792.
40 E. S. S. Iyer, A. Sadybekov, O. Lioubashevski, A. I. Krylov and S. Ruhman, J. Phys. Chem. A, 2017, 121, 1962–1975.
41 Y. Wu, J. Zhou, B. T. Phelan, C. M. Mauck, J. F. Stoddart, R. M. Young and M. R. Wasielewski, J. Am. Chem. Soc., 2017, 139(40), 14265–14276.
42 M. Koch, G. Licari and E. Vauthey, J. Phys. Chem. B, 2015, 119, 11846–11857.
43 B. Dereka, M. Koch and E. Vauthey, Acc. Chem. Res., 2017, 50, 426–434.